Acta Cryst. (1965). **18**, 37

Neutron Diffraction Studies of the Order of the Atoms in the *P* Phase and the *R* Phase*

By Clara B. Shoemaker, David P. Shoemaker and John Mellor

Department of Chemistry, Massachusetts Institute of Technology, Cambridge 39, *Massachusetts, U.S.A.*

(*Received* 6 *January* 1964)

The ordering of the atoms in two ternary alloys, *P* phase (Mo–Ni–Cr) and *R* phase (Mo–Fe–Mn), both structurally related to the σ phase, has been studied by powder neutron diffraction. The at.% Mo on each site was taken to be approximately that determined in previous X-ray single-crystal studies, which showed that Mo preferentially occupies CN16 and CN15 sites. From the best fit between observed and calculated neutron diffraction diagrams it is apparent that, in the *P* phase, Ni preferentially occupies CN12 positions. In the *R* phase, Mn shows only a slight preference for CN14 and CN15 positions over CN12 positions when competing with Fe. The results are consistent with those of ordering studies of related transition element intermetallic compounds.

Introduction

In our single-crystal X-ray diffraction studies of the *P* phase, occurring in the Mo–Ni–Cr system (Shoemaker, Shoemaker & Wilson, 1957), and of the *R* phase, occurring in the Mo–Co–Cr system (Komura, Sly & Shoemaker, 1960), we found evidence of considerable ordering. The approximate percentage of Mo on each site could be determined, but the two lighter atoms have scattering factors for X-rays that are so closely similar that they cannot be distinguished by means of X-ray diffraction. Moreover, in a three-component partially disordered phase, two parameters are required to determine the composition of each site (assuming that there are no vacancies), and an X-ray electron count provides only one.

In some cases where similarity of X-ray scattering factors has made determination of order with X-rays difficult, neutron diffraction has been used. Several σ phases (Kasper & Waterstrat, 1956), and a χ phase (Kasper, 1954) have been investigated. In the present investigation we employed neutron diffraction in a further study of order in the *P* and *R* phases. For the *P* phase, the scattering factors for neutrons are quite different for Ni and Cr (1·03 and $0{\cdot}35\times10^{-12}$ cm respectively) and the distribution of these elements may thus be determined by neutron diffraction once the Mo occupancy is approximately known from X-rays. This is not true for Co and Cr in the Mo–Co–Cr *R* phase; the neutron scattering factors for Co and Cr are not very different (0·28 and $0{\cdot}35\times10^{-12}$ cm respectively). However, the *R* phase also occurs in the Mo–Fe–Mn system, and Fe and Mn differ considerably in neutron scattering factor (0·96 and $-0{\cdot}37\times10^{-12}$ cm respectively). Accordingly, we chose *P*(Mo–Ni–Cr; 39:37:24 atom ratio) and *R*(Mo–Fe–Mn; 32:52:16) for our neutron diffraction study. Since the crystals of these alloys are far too small for neutron diffraction single-crystal work, powdered materials were used. The complexity of the *P* and the *R* phase structures results in considerable overlap of reflections in their powder X-ray and neutron diffraction diagrams, particularly in the latter because of the larger wavelength spread in the neutron beam. It was therefore necessary to develop computational procedures for dealing with unresolved powder lines.

Experimental

The two alloys were prepared in the laboratory of Prof. Paul A. Beck, University of Illinois, by arc fusion of the mixed pure metals in the proportions above stated followed by annealing at 1200 °C. For the diffraction work we used 20-g samples that passed through a 100 mesh sieve. The neutron diffraction powder intensities were measured at the M.I.T. nuclear reactor on the powder spectrometer (S2) built by Prof. C. G. Shull and used by arrangement with him. A lead monochromator crystal was used, adjusted to give a peak wavelength of 1·2085 Å. The sample holder was a thin-wall vanadium cylinder with a radius of 5 mm. The sample was rotated to avoid intensity variation due to graininess. Counts were taken at intervals of 0·05° in 2θ. With a 600,000 monitor count, the background was about 250–300 counts for the *P* phase and about 150–200 counts for the *R* phase. The peaks at 32° were about 650 counts amplitude at maximum for both alloys.

The scatter in the neutron spectrometer counts was reduced by a smoothing program written for the IBM 709 computer. The smoothing was done by convolution of the intensity function at 0·05° intervals with a sequence of eight binomial coefficients (1, 7, 21, 35, 35, 21, 7, 1), and resulted in reduction of the squared standard error for the smoothed intensity at each scattering angle to about one fifth the value

* Sponsored by Army Research Office (Durham). Computations done at the MIT Computation Center.

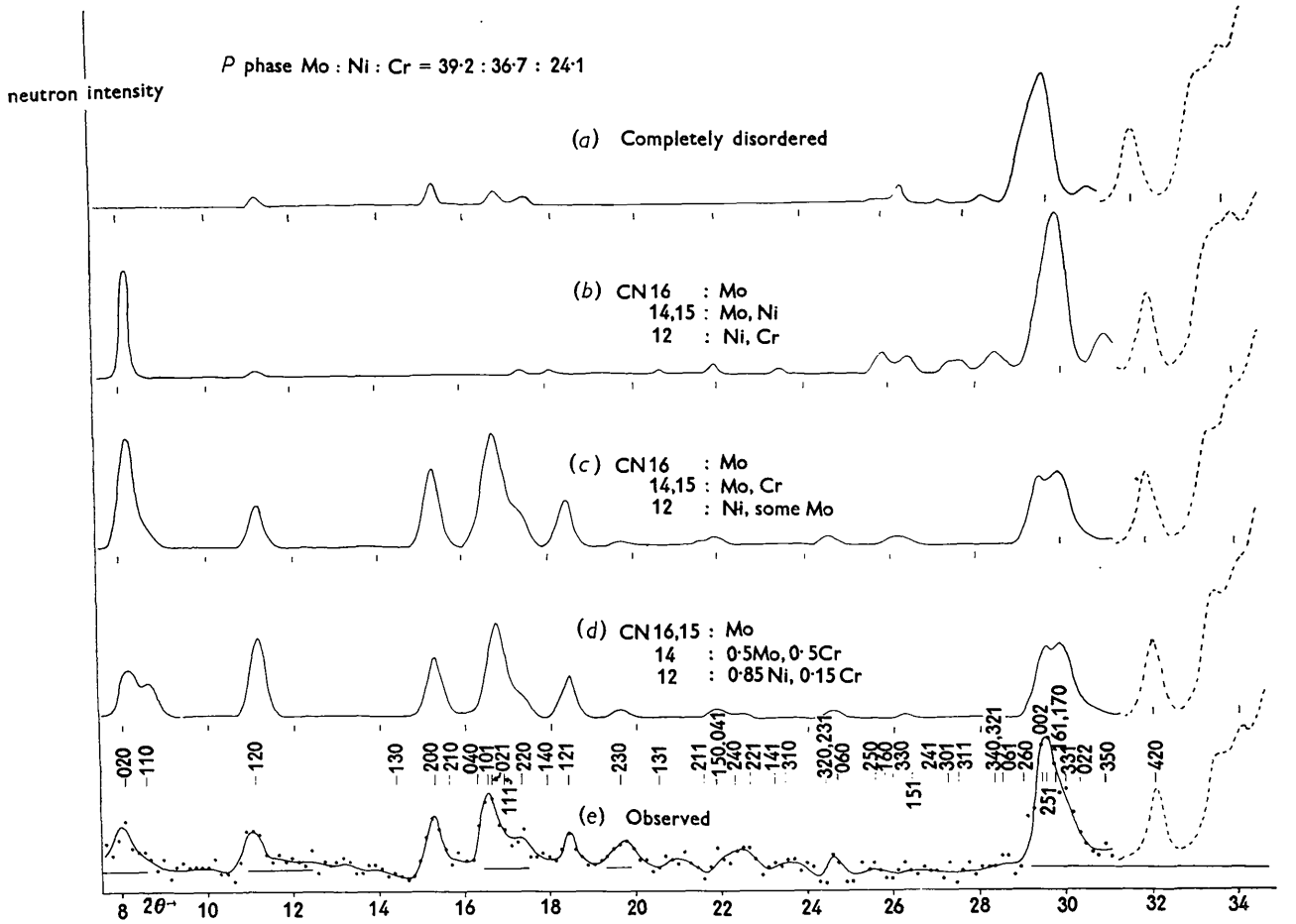

Fig. 1. *P* phase: observed (*e*) and calculated neutron diffraction powder diagrams for four different distributions of the atoms (*a*), (*b*), (*c*), (*d*). The labels give the approximate values for these distributions; the actual compositions used in the calculation of the diagrams are given in Table 1. Intensity scale is reduced 4:1 in dashed parts of the curves. Curves were drawn in by hand through points on computer output sheets. Two-degree markers are given for each curve. (Slight variation in marker spacings reflects some variation in output-printer spacings.) Wavelength for all diagrams is 1·2085 Å.

for the unsmoothed intensity, without broadening the peaks appreciably. The background was not constant and was approximated by a power series in 2θ with four coefficients. The resulting values, corrected for the background, were plotted (as decimal points on IBM output sheets with a subroutine, PRPLOT) at 0·15° intervals in 2θ. The intensity plots are shown at the bottoms of Figs. 1 and 2.

Computed diffraction diagrams

The intensity at each diffracting angle 2θ was calculated by adding the contributions at 2θ of all neighbouring lines:

$$I(2\theta)=K.L(2\theta).\sum_{hkl} m(hkl).F^2(hkl).S(2\theta_{hkl}-2\theta,2\theta) \quad (1)$$

where

K = scale factor,
L = Lorentz factor modified for powder diffraction $=1/(\sin\theta.\sin 2\theta)$,
m = powder multiplicity,
$S(2\theta_{hkl}-2\theta, 2\theta)$ = contribution of reflection hkl to intensity at 2θ (shape function), and
F = structure factor, including temperature factor.

The structure factors were calculated assuming the atomic positional parameters determined in the single crystal X-ray studies (Shoemaker *et al.*, 1957; Komura *et al.*, 1960). These parameters may deviate slightly from those of the present alloys owing to the different compositions, but such deviations are not expected to affect the structure factors much at the low angles used (7°–32° in 2θ). No absorption correction was applied since μR was about 0·2 and the absorption in this 2θ range can therefore be assumed to be essentially constant.

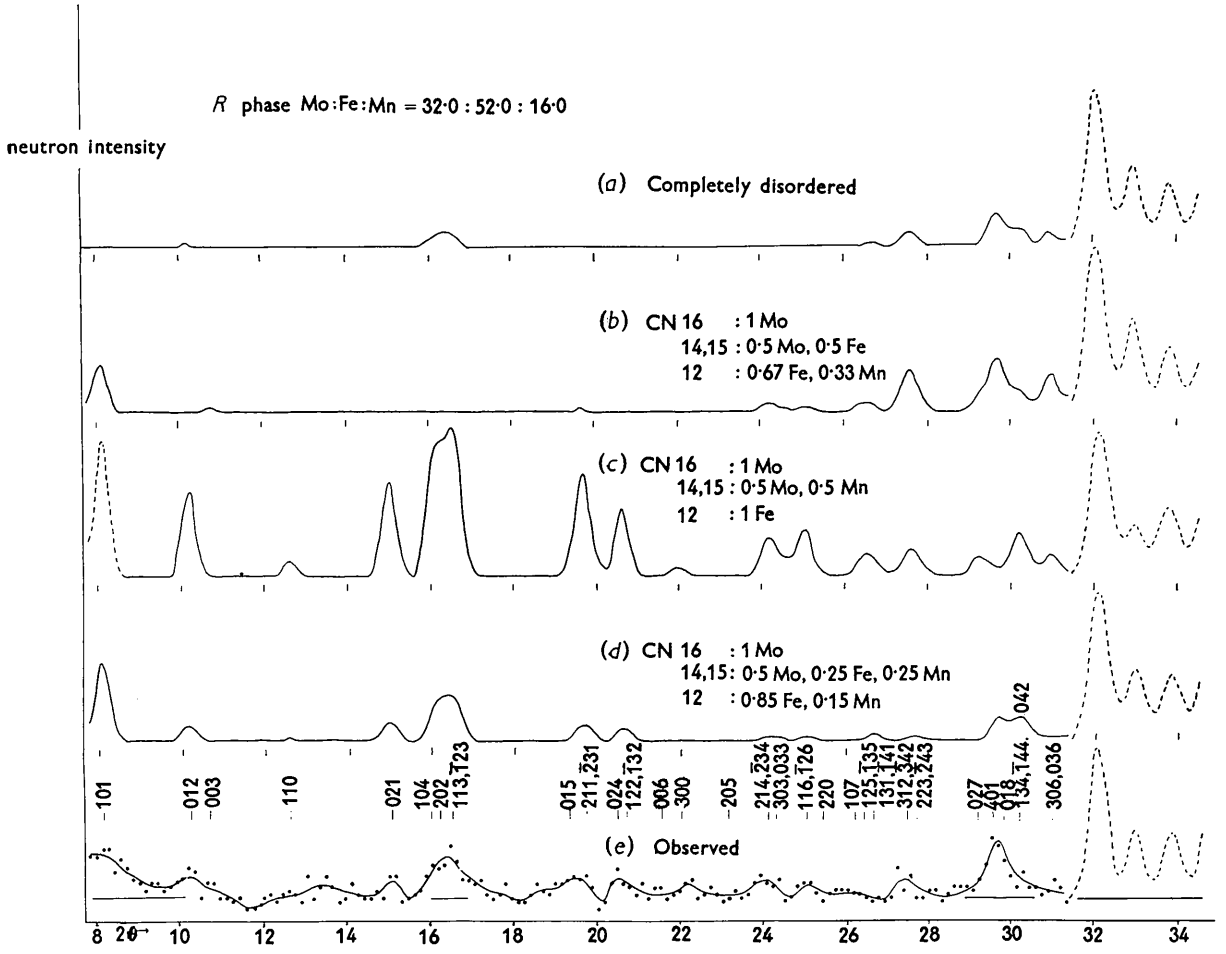

Fig. 2. *R* phase: observed (*e*) and calculated neutron diffraction powder diagrams for four different distributions of the atoms (*a*), (*b*), (*c*), (*d*). The actual compositions used in the calculation of the diagrams are given in Table 2. Intensity scale is reduced 4:1 in dashed parts of the curves. Wavelength for all diagrams is 1·2085 Å.

The peak shape function S in a neutron diffraction diagram is an explicit function of 2θ because of the rather large wavelength spread in the neutron beam. A nickel powder (particles smaller than 100 mesh) which showed very nearly Gaussian powder diffraction peaks was used to obtain a curve of the Gaussian parameter $\sigma(2\theta)$ as a function of 2θ. However the first Ni peak is at about $2\theta=34°$ and we are concerned with the diffraction pattern at angles less than 34°. There is only one well resolved P phase peak (420) of high intensity in this region (the intensity of the coinciding reflection 341 is less than 4% of the intensity of 420), and four (120, 200, 121, and 230) that are fairly well resolved but have very low intensity. With the aid of the (not very accurate) σ values for these peaks the σ *versus* 2θ curve was plotted and extrapolated to $2\theta=0°$ (Fig. 3). This curve was used in the calculation of the Gaussian shape function by the computer program:

$$S(2\theta_{hkl}-2\theta,\ 2\theta) = \frac{1}{\sqrt{2\pi}\sigma(2\theta)} \exp\left\{-(2\theta_{hkl}-2\theta)^2/2[\sigma(2\theta)]^2\right\}. \quad (2)$$

The X-ray powder diffraction diagrams of both the P and the R phases (like those of σ and similar phases) have large regions of low intensity alternating with regions where strong lines are grouped closely together. In the neutron powder diffraction diagrams the first high intensity region starts at about $2\theta=32°$. The intensities of the strong lines are relatively insensitive to changes in atomic distribution and the intensities of the lines at $2\theta=32°$ were used to determine the scale factors K in equation (1).

The computer program for calculating the intensities determined at each 2θ value what lines contributed to the intensity, then calculated and added these contributions. The neutron scattering factors used in the calculations were:

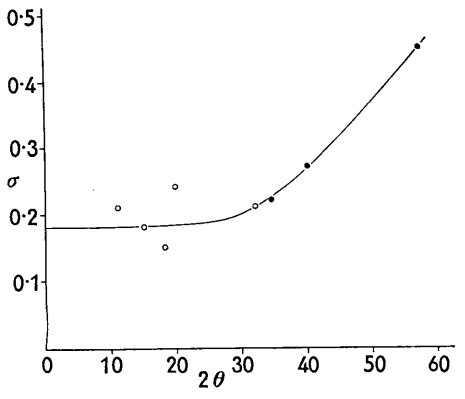

Fig. 3. Curve of Gaussian parameter σ *versus* 2θ in degrees. Open circles apply to *P* phase reflections 120, 200, 121, 230, 420 in that order; closed circles apply to Ni reflections 111, 200, 220.

Mo	$0{\cdot}66\times10^{-12}$ cm
Ni	1·03
Cr	0·35
Fe	0·96
Mn	−0·37

(These differ negligibly, for our present purpose, from improved values that have since been published.) The X-ray over-all isotropic temperature factors of 1·1 Å^2 for the *P* phase and 0·67 Å^2 for the *R* phase were assumed. The results were plotted (with the aid of the subroutine PRPLOT) for comparison with the observed intensity functions.

The IBM 709 computer program was originally written for a least-squares refinement of the differences between observed and calculated intensities with the scattering factors and temperature factors as parameters. This part of the program did not give meaningful results, probably because there are not enough diffraction lines of sufficient intensity above the high background in the useful low-angle region of the neutron-diffraction diagrams. Thus, we were obliged to confine ourselves to the calculating and testing of a limited number of models of atomic ordering.

Results

P phase

Crystal data for the *P* phase as obtained in the prior X-ray study (Shoemaker *et al.*, 1957) are as follows:

Space group: *Pbnm* (D_{2h}^{16}), $Z=56$ atoms per cell.
$a_0=9{\cdot}070$, $b_0=16{\cdot}983$, $c_0=4{\cdot}752$ Å.
Atom ratio Mo:Ni:Cr = 42:40:18.

The percentages of Mo on the various sites were estimated in the X-ray study from the contents of the peaks in the generalized electron density projection. This could not be done very accurately; the limits of error were estimated at about 30% in the figures for per cent Mo. These estimated percentages had to be adjusted to give the correct overall percentage of Mo in the alloy used in the present study (Mo : Ni : Cr = 39·24 : 36·66 : 24·10 by synthesis, or 22·0 Mo, 20·5 Ni, 13·5 Cr per unit cell). The estimated percentages of Mo arrived at are listed in the fifth column of Table 1. Probably the value of 100% for position 7 is too high and that for position 5 too low by as much as 25% or more. However, these listed percentages of Mo were the ones actually used in two of the four models illustrated (*b* and *c*).

The lattice constants obtained in the X-ray work were used in the present work, as inspection of the powder diagrams showed negligible shifts.

Fig. 1 shows four calculated diffraction diagrams together with the observed diagram, obtained after smoothing and subtracting of the background. The curves were drawn by hand through the points on the IBM output sheets produced by the subroutine PRPLOT. The compositions and the scattering factors for the different models tested are given in Table 1.

Curve (*a*) is calculated for a completely disordered structure with *b* for all atoms = 0·72. There is very

Table 1. *Compositions and neutron scattering factors for P-phase models used in Fig.* 1

Site No.	CN	Atom mult.	X-ray % Mo	*Assumed % Mo	(*b*) % Ni	(*b*) % Cr	(*b*) *b*	(*c*) % Ni	(*c*) % Cr	(*c*) *b*	(*d*) % Mo	(*d*) % Ni	(*d*) % Cr	(*d*) *b*
1	12	4	35	18	37	45	0·66	73	9	0·90		85	15	0·93
2	12	4	20	18	37	45	0·66	73	9	0·90		85	15	0·93
3	12	4	0	0	37	63	0·60	91	9	0·97		85	15	0·93
8	12	4	<0	0	37	63	0·60	91	9	0·97		85	15	0·93
11	12	8	<0	0	37	63	0·60	91	9	0·97		85	15	0·93
4	14	4	78	50	50		0·84		50	0·50	50		50	0·51
7	14	4	100	100(?)			0·66			0·66	50		50	0·51
9	14	4	78	50	50		0·84		50	0·50	50		50	0·51
12	14	8	52	38	62		0·89		62	0·47	50		50	0·51
5	15	4	65	38(?)	62		0·89		62	0·47	100			0·66
10	15	4	>100	100			0·66			0·66	100			0·66
6	16	4	>100	100			0·66			0·66	100			0·66

* Assumed value for models (*b*) and (*c*), adjusted downwards to give correct overall % Mo for the alloy used in the present study.

Table 2. *Compositions and neutron scattering factors for R-phase models used in Fig. 2*

Site No.	CN	Atom mult.†	X-ray % Mo	*Assumed % Mo	(b) % Fe	(b) % Mn	(b) b	(c) % Fe	(c) % Mn	(c) b	(d) % Mo	(d) % Fe	(d) % Mn	(d) b
*A*1	12	3	11	8	61	31	0·52	92		0·94		85	15	0·76
*A*2	12	6	0	0	68	32	0·54	100		0·96		85	15	0·76
*A*3	12	18	0	0	68	32	0·54	100		0·96		85	15	0·76
*A*4	12	18	0	0	68	32	0·54	100		0·96		85	15	0·76
*A*5	12	18	11	8	61	31	0·52	92		0·94		85	15	0·76
*A*6	12	18	0	0	68	32	0·54	100		0·96		85	15	0·76
*B*1	14	18	62	42	58		0·83	6	52	0·14	50	25	25	0·48
*B*2	14	18	53	42	58		0·83	6	52	0·14	50	25	25	0·48
*C*1	15	18	76	55	45		0·79	6	39	0·28	50	25	25	0·48
*D*1	16	6	>100	100			0·66			0·66	100			0·66
*D*2	16	18	100	100			0·66			0·66	100			0·66

* Assumed value for models (*b*) and (*c*), adjusted downward to give correct overall % Mo for the alloy used in the present study.
† Per hexagonal cell.

little intensity variation below $2\theta = 29°$ predicted by this model.

Model (*b*) has Mo distributed as described above, all Cr in CN12 positions, and Ni in the remaining CN12, 14, 15 positions. This model does not predict appreciable intensity between $2\theta = 14$ and 20°.

Model (*c*) has the same Mo distribution as model (*b*), but all Ni in CN12 positions and Cr in the remaining CN12, 14, 15 positions. This curve agrees rather well with the observed curve, but the peak at 8° is too high, and the peak at 29·5° is too low.

Model (*d*) has the same occupancy for all atoms of the same coordination number. All Mo has been taken out of the CN12 positions and has been replaced by Cr. CN15 and 16 are occupied by Mo and CN14 by 0·5 Mo and 0·5 Cr. The peak at $2\theta = 8°$ is now lower, otherwise curve (*d*) is very similar to curve (*c*), and the peak at 2θ about 30° still has the wrong shape.

Although none of the models faithfully reproduces all of the features of the experimental curve, it is clear that models (*a*) and (*b*) are ruled out and model (*d*) gives the best fit. Comparison of the smaller features is difficult because of the scatter in the experimental points. In addition, contribution of lines from low level impurities cannot be ruled out in view of the general weakness of all powder lines in this region. All models fail to account properly for the relatively high peak at 29·5°. A half-wavelength contribution from the very strong 004 is expected in this region but cannot explain more than a fraction of the discrepancy. All models yield peaks at 30° which are too high by comparison with a shoulder that appears on the experimental curve; however, models (*c*) and (*d*) are superior to models (*a*) and (*b*) in this regard.

Several other models were tried in attempts to improve specific features but none gave fits better than that shown for model (*d*). In view of our failure to obtain meaningful results with a least-squares procedure, the conclusions to be reached from these results must be limited to stating that the nickel atoms have a decided preference for the CN12 sites, the Mo atoms prefer the CN16 and CN15 sites, and some mixtures of Mo and Cr predominate in the CN14 sites.

R phase

Crystal data for the *R* phase as obtained in the prior X-ray study (Komura *et al.*, 1960) are as follows:

Space group: $R\bar{3}$ (C_{3i}^2), $Z = 3 \times 53$ atoms per hexagonal cell,
$a_0 = 10{\cdot}903$, $c_0 = 19{\cdot}342$ Å (hexagonal),
Atom ratios Mo:Co:Cr = 30·4:51·3:18·3.

The percentages of Mo on each site were estimated in the X-ray study by a least-squares analysis carried out with a modification of the IBM 704 program NYXR 1, in which the atomic positions and the scattering factors were varied simultaneously, but the temperature factors kept constant. These figures should be more accurate than the figures obtained for the *P* phase from the Fourier syntheses, but they are dependent on the temperature factors assumed for the individual atoms, and closely coupled with them. The Mo percentages in the Mo–Fe–Mn *R* phase used in the neutron work were adjusted from those found in the Mo–Co–Cr *R* phase to give the correct overall percentage of Mo in the alloy used in the present study (Mo:Fe:Mn = 32:52:16, or 3×17 Mo, $3 \times 27{\cdot}5$ Fe, and $3 \times 8{\cdot}5$ Mn per unit cell). The estimated percentages of Mo arrived at are listed in the fifth column of Table 2, and were used in two of the four models illustrated (*b* and *c*).

For the Mo–Fe–Mn *R* phase the following (hexagonal) cell dimensions were determined by least-squares analysis of X-ray powder data:

$$a_0 = 10{\cdot}983,\ c_0 = 19{\cdot}398\ \text{Å}.$$

The curves obtained for the *R* phase are shown in Fig. 2 and the compositions of the *R*-phase models are given in Table 2.

Model (*a*) is a completely disordered structure

with $b=0{\cdot}65$ for every position. There is again very little intensity variation predicted by this model for 2θ less than 30°. The diffraction diagram would be essentially the same for a model which had Mo in the positions deduced from the X-ray study and Fe and Mn distributed at random over the remaining positions.

Model (*b*) has Mo distributed as described above, all Mn in CN12 and Fe in the remaining CN12, 14, 15 positions. This model does not predict appreciable intensity between $2\theta=14$ and 18°.

Model (*c*) has the same Mo distribution as model (*b*), but Mn is confined to CN14 and 15, and CN12 is mainly occupied with Fe. This model predicts a very high peak at $2\theta=8°$, which was not observed, and most other peaks with 2θ less than 30° are much too high. However, they do correspond roughly to features of the observed diagram. Apparently some Mn must occupy CN12 positions.

Model (*d*) has no Mo in CN12, CN16 positions contain 100% Mo, CN14 and 15 contain 50% Mo, 25% Fe and 25% Mn, and CN12 positions contain 85% Fe and 15% Mn. The agreement with the observed curve is now fairly good, except for 2θ about 29·5–31°. This is the same region where the *P* phase model (*d*) shows the largest deviations from the observed curve.

The assumption that the ordering of Mo is approximately the same in Mo–Mn–Fe as in Mo–Co–Cr, except as regards over-all Mo content, is a reasonable one owing to the comparatively large size of Mo. From this study one cannot exclude considerable mixture of Mo with Fe, but this appears very unlikely except perhaps in CN14 and CN15. Admixture of Mo with Mn to a degree very different from model (*d*) can be excluded since Mo and Mn have very different scattering factors.

Discussion

The results obtained are in agreement with the conclusions reached previously by Kasper & Waterstrat (1956) for the σ phases: the elements to the left of the Mn column in the periodic table (A elements: Mo, Cr) prefer the higher coordinated positions (CN16, CN15), the elements to the right of Mn (B elements: Fe, Ni) prefer the CN12 positions, and mixtures of the two groups of elements occupy the CN14 (and CN15) positions. Mn itself behaves as A or B element depending on the element(s) it is alloyed with. In the *R* phase Mn shows only a slight preference for CN14 and CN15 over CN12 when competing with Fe.

Tables 3 and 4 give the results of ordering studies of several transition element intermetallic compounds to which the *P* and *R* phases are related. The ordering

Table 3. *Results of ordering studies of related transition element intermetallic compounds not containing* Mn *or* Re

(These vary considerably in precision)

Phase	At.% A	Atomic percentages A on sites*					Method
		CN16	CN15	CN14	CN13	CN12	
Laves phases							
AB_2	33	100				0	X-ray‡
χ phase							
$Mo_{10}Cr_{12}Fe_{36}$	38	100 Mo			38 Cr	12 Cr	Powder neutron (1)
μ phase							
Mo_6Co_7	46	100	100	100		0	Single crystal X-ray (2)
δ phase							
MoNi	50	100	100	58, 80, 91		0	Single crystal X-ray (3)
P phase							
$Mo_{39}Cr_{24}Ni_{37}$	63	100	100	50 Mo + 50 Cr		15 Cr	Single crystal X-ray and powder neutron (4)
σ phases†							
MoFe	50		75	75		0	Powder X-ray (5)
$V_{17}Ni_{13}$	57		100	62, 100		0	Powder neutron (6)
$V_{18}Fe_{12}$	60		100	81, 75		15, 15	Powder neutron (6)
Mo_3Co_2	60		100	88		0	Single crystal X-ray (7)
$V_{19}Ni_{11}$	63		100	81, 99		10, 9	Powder neutron (6)
$V_{21}Ni_9$	70		98	94, 99		15, 14	Powder neutron (6)
β–W phases							
A_3B	75			100		0	X-ray‡

* Atomic percentages of B are 100 minus atomic percentages of A given. Blanks indicate that such coordinations are not present in the structure. Differing values for different sites of same CN are separated by commas.

† Waterstrat & Kasper (1957) have reported completely disordered structures for Os–Cr and Ru–Cr σ phases.

‡ Generally completely ordered as indicated by composition.

(1) Kasper, 1954
(2) Forsyth & d'Alte da Veiga, 1962
(3) Shoemaker & Shoemaker, 1963
(4) This study
(5) Wilson & Spooner, 1963
(6) Kasper & Waterstrat, 1956
(7) Forsyth & d'Alte da Veiga, 1963

Table 4. *Results of ordering studies of related transition element intermetallic compounds containing* Mn *or* Re

(These vary considerably in precision)

Phase	At.% A	At.% Mn or Re	Atomic percentages on sites*					Method
			CN16	CN15	CN14	CN13	CN12	
χ phases								
Re_4Mn_{54}		7 Re + 93 Mn	20 Re			4 Re	4 Re	Powder X-ray (1)
$Ti_{10}Re_{48}$	17 Ti	83 Re	100 Ti			0 Ti	0 Ti	Powder X-ray (2)
$Mo_{10}Re_{48}$	17 Mo	83 Re	100 Mo			0 Mo	0 Mo	Powder X-ray (3)
$Re_{18}Fe_{40}$		31 Re	100 Re			33 Re	0 Re	Powder X-ray (4)
Mn_7Fe_3		70 Mn	100 Mn			75 Mn	50 Mn	Powder neutron (5)
R phase								
$Mo_{32}Mn_{16}Fe_{52}$	32 Mo	16 Mn	100 Mo	50 Mo + 25 Mn	50 Mo + 25 Mn		15 Mn	Single crystal X-ray and powder neutron (6)
σ phases								
$CrMn_3$	25 Cr	75 Mn		25 Cr	37 Cr, 44 Cr		0 Cr	Powder neutron (7)
$Mo_{12}Mn_{18}$	40 Mo	60 Mn		100 Mo	50 Mo		0 Mo	Powder X-ray (8)
$Cr_{12}Re_{18}$†	40 Cr	60 Re		100 Cr	0 Cr, 100 Cr		0 Cr	Powder X-ray (9)
$Re_{12}Fe_{18}$		40 Re		100 Re	50 Re		0 Re	Powder X-ray (9)
$Mo_{10}Re_{20}$	32 Mo	68 Re		50 Mo	50 Mo		0 Mo	Powder X-ray (10)
$Mo_{12}Re_{18}$	40 Mo	60 Re		100 Mo	0 Mo, 100 Mo		0 Mo	Powder X-ray (3)
$Mo_{13\cdot5}Re_{16\cdot5}$	45 Mo	55 Re		75 Mo	50 Mo, 62 Mo		0 Mo, 19 Mo	Powder X-ray (10)
$Re_{16}Mn_{14}$		53 Re + 47 Mn		100 Re	75 Re		0 Re	Powder X-ray (9)

* Atomic percentages of remaining constituent are 100 minus atomic percentages of constituent(s) given. Blanks indicate that such coordinations are not present in the structure. Differing values for different sites of same CN are separated by commas.

† Waterstrat & Kasper (1957) have reported a completely disordered structure for a Re_2Cr σ phase.

(1) Ageev & Shekhtman, 1962*a*
(2) Trzebiatowski & Niemic, 1955
(3) Ageev & Shekhtman, 1959
(4) Ageev & Shekhtman, 1962*b*
(5) Kasper, 1956
(6) This study
(7) Kasper & Waterstrat, 1956
(8) Decker, Waterstrat & Kasper, 1954
(9) Ageev & Shekhtman, 1960
(10) Wilson, 1963

parameters obtained in our study of the *P* and *R* phases are less precise and less reliable than those obtained by Kasper & Waterstrat in their neutron diffraction studies of σ and χ phases. This is due in large part to the greater complexity of the *P* and *R* phases and the resulting less favorable peak intensity to background ratio.

The results summarized in Table 4 indicate that Re has a dual character like Mn, behaving as A element in some phases and as B element in others. There are, however, some differences in detail in the distributions of the atoms, particularly in the CN14 positions, obtained by different authors.

Assuming that only A elements occupy CN15 and CN16 positions and only B elements CN12 positions and a mixture of A and B elements CN13 or CN14 positions, one can predict possible composition limits for the various phases. Table 5 shows that wide composition ranges are possible consistent with this assumption. In practice the composition of these phases is usually restricted (presumably by valence electron concentration) to a very narrow field (see compilation by Nevitt, 1963, pp. 106, 113, 118), which generally lies within the broad limits predicted by Table 5. Notable exceptions are Ta σ phases

Table 5. *Predicted composition limits, assuming only* A *elements in* CN16 *and* CN15, *only* B *in* CN12

Phase	Percentages of sites with CN15 and CN16	CN14	CN13	CN12	Predicted limits, at.% A
χ	17		41	41	17–58
μ	30	15		55	30–45
R	26	22		52	26–48
δ	21	36		43	21–57
P	21	36		43	21–57
σ	13	53		33	13–66

containing as B elements Pd, Os, Ir or Pt; their σ phase fields lie completely outside the predicted range (*e.g.* TaIr σ, 75–85% Ta), indicating that some Ta also has to occupy CN12 positions. One of the VNi σ phases quoted in Table 3 ($V_{21}Ni_9$) contains more V than is consistent with the assumptions of Table 5. The neutron diffraction studies (Kasper & Waterstrat, 1956) indicated that some V occupies CN12 positions and this was also found for one composition of this phase that is within the composition limits of Table 5. The *P* phase investigated in this study does not contain enough Ni to occupy completely the CN12 positions; some Cr must be present in these positions. The results are however not precise enough to exclude the possibility that some Mo is also present in these positions. Several phases listed by Nevitt (1963) in which Mn, Tc, or Re is the B component contain less A component than is necessary to fill up the available CN15 and CN16 positions; thus, Mn, Tc and Re also occupy A positions to some extent.

Although in the more complicated phases a mixture of A and B elements occupies the CN14 positions, this does not seem to apply to the β-W phases, which have been reported generally at exact composition A_3B, with A occupying CN14 and B occupying CN12 positions. That the Laves phases occur at exact compositions, AB_2, is less surprising since the coordinations are so different (CN16 and CN12).

It is a pleasure to thank Prof. Paul A. Beck of the University of Illinois for supplying us with the specimens and Prof. C. G. Shull for the use of his neutron diffraction equipment.

We gratefully acknowledge financial support from the U.S. Army Research Office (Durham), and the use of the facilities of the M.I.T. Computation Center.

References

Ageev, N. V. & Shekhtman, V. Sh. (1959). *Acad. Sci. USSR*, Bulletin **23**, 650.

Ageev, N. V. & Shekhtman, V. Sh. (1960). *Dokl. Akad. Nauk SSSR*, **135**, 309.

Ageev, N. V. & Shekhtman, V. Sh. (1962*a*). *Dokl. Akad. Nauk SSSR*, **143**, 922.

Ageev, N. V. & Shekhtman, V. Sh. (1962*b*). *Dokl. Akad. Nauk SSSR*, **143**, 1091.

Decker, B. F., Waterstrat, R. M. & Kasper, J. S. (1954). *Trans. Amer. Inst. Min. (metall) Engrs*, **200**, 1406.

Forsyth, J. B. & da Veiga, L. M. d'Alte (1962). *Acta Cryst.* **15**, 543.

Forsyth, J. B. & da Veiga, L. M. d'Alte (1963). *Acta Cryst.* **16**, 509.

Kasper, J. S. (1954). *Acta Met.* **2**, 456.

Kasper, J. S. (1956). In *Theory of Alloy Phases*. Cleveland: American Society for Metals.

Kasper, J. S. & Waterstrat, R. M. (1956). *Acta Cryst.* **9**, 289.

Komura, Y., Sly, W. G. & Shoemaker, D. P. (1960). *Acta Cryst.* **13**, 575.

Nevitt, M. V. (1963). In *Electronic Structure and Alloy Chemistry of the Transition Elements* (P. A. Beck, ed.). New York: Wiley, Interscience Monograph Series.

Shoemaker, D. P., Shoemaker, C. B. & Wilson, F. C. (1957). *Acta Cryst.* **10**, 1.

Shoemaker, C. B. & Shoemaker, D. P. (1963). *Acta Cryst.* **16**, 997.

Trzebiatowski, W. & Niemic, J. (1955). *Roczniki Chem.* **29**, 277.

Waterstrat, R. M. & Kasper, J. S. (1957). *Trans. Amer. Inst. Min. (metall) Engrs*, **209**, 872.

Wilson, C. G. & Spooner, F. J. (1963). *Acta Cryst.* **16**, 230.

Wilson, C. G. (1963). *Acta Cryst.* **16**, 724.